

NMR solution structure of the periplasmic chaperone FimC

The NMR structure of the 205-residue periplasmic chaperone FimC is presented. This protein consists of two globular domains with immunoglobulin-like folds connected by a 15-residue linker peptide. The relative orientation of the two domains is defined by hydrophobic contacts and an inter-domain salt bridge. FimC mediates the assembly of type-1 pili, which are filamentous surface organelles of uropathogenic *Escherichia coli* strains that enable the bacteria to attach to host cell surfaces and persist in macrophages. The availability of the NMR structure of FimC provides a new basis for rational design of drugs against infections by uropathogenic bacteria.

A key event in infections by pathogenic Gram-negative enterobacteria is attachment to host cell receptors. This process is mediated by adhesive surface organelles, the so-called pili or fimbriae^{1–11}. Pili are large, hetero-oligomeric protein filaments anchored to the bacterial outer membrane. Type-1 pili are present in virtually all uropathogenic *E. coli* strains that cause cystitis and are required for efficient bladder colonization¹⁰. They enable the bacteria to bind to mannose-containing structures of host cell surfaces and support their survival inside

macrophages by enabling the bacteria to become internalized through a non-phagocytic pathway³.

Type-1 pili are composed of up to 1,000 protein subunits, which form filaments that are ~1 μm long and ~7 nm wide¹. FimA, the main structural subunit of the pili, accounts for ~98% of the pilus protein, while FimI, FimF, FimG and the mannose-binding subunit FimH account for the residual 2%¹. Assembly of the pilus *in vivo* is mediated by the periplasmic chaperone FimC, which is a soluble monomeric protein of 205 amino acids^{4,5}. Biochemical, structural and genetic studies on the assembly of type-1 pili, the related P-pili from *E. coli*, and many adhesive pili from other bacteria led to the hypothesis that the periplasmic chaperones recognize the highly conserved C-terminal peptide segments of the different subunits, form stoichiometric complexes with folded forms of the subunits in the periplasm, and deliver the subunits to an assembly platform protein in the outer bacterial membrane^{2,6,7}. Thus, although most common chaperones interact with unfolded or partially folded polypeptides and inhibit protein aggregation during protein folding⁸, FimC and all other members of the periplasmic pilus chaperone family appear to recognize folded forms of the pilus subunits and prevent their spontaneous aggregation in the periplasm.

As type-1 pili enhance the virulence of pathogenic *E. coli* cells^{3,9} they are potential targets for antibiotics that may either prevent the assembly of the pili or inhibit adhesiveness. In addition, the FimC–FimH complex has proved to be a promising vaccine against mucosal *E. coli* infections¹⁰. As a further step toward elucidation of the molecular events underlying the

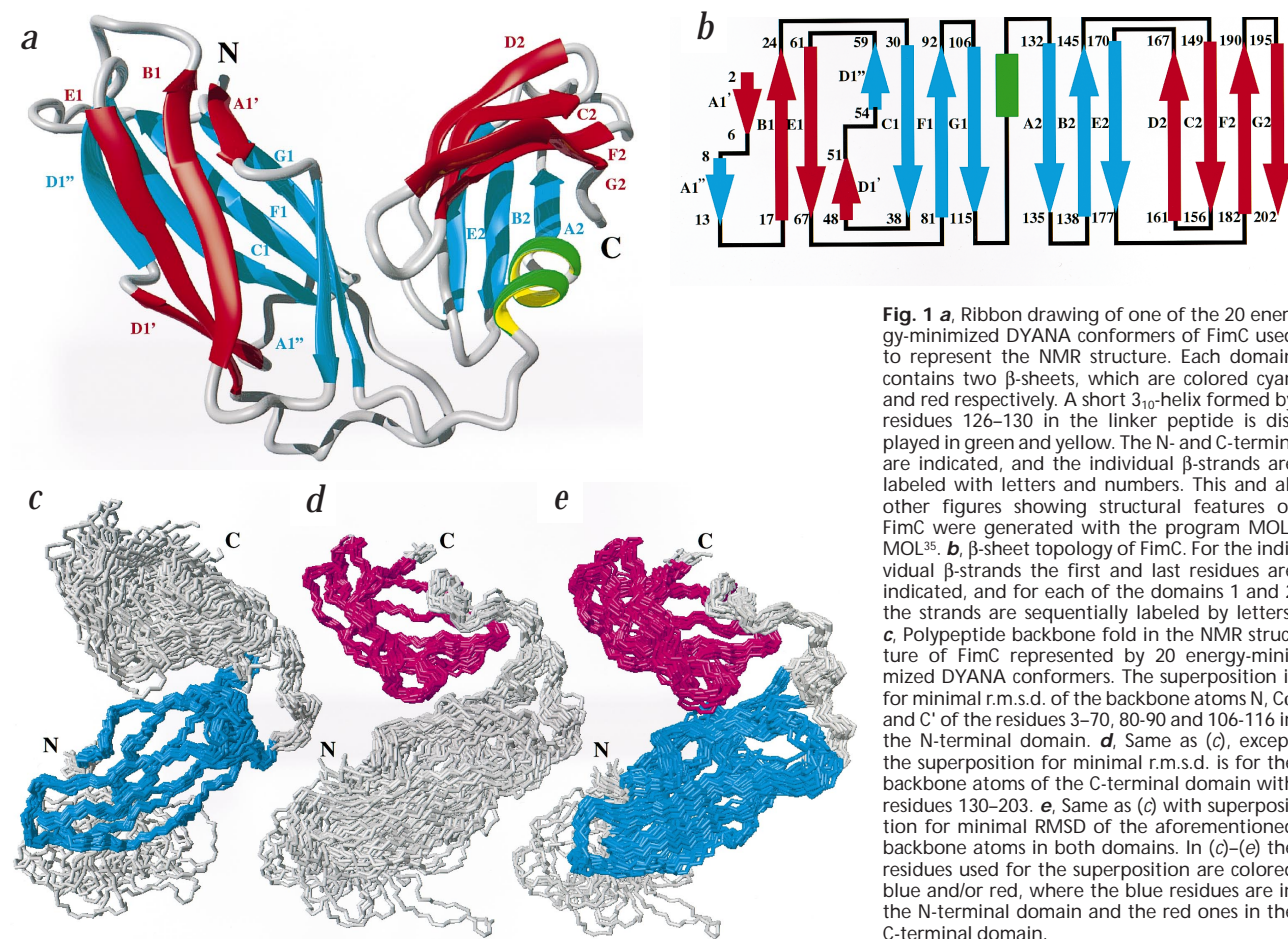


Fig. 1 **a**, Ribbon drawing of one of the 20 energy-minimized DYANA conformers of FimC used to represent the NMR structure. Each domain contains two β-sheets, which are colored cyan and red respectively. A short 3₁₀-helix formed by residues 126–130 in the linker peptide is displayed in green and yellow. The N- and C-termini are indicated, and the individual β-strands are labeled with letters and numbers. This and all other figures showing structural features of FimC were generated with the program MOLMOL³⁵. **b**, β-sheet topology of FimC. For the individual β-strands the first and last residues are indicated, and for each of the domains 1 and 2 the strands are sequentially labeled by letters. **c**, Polypeptide backbone fold in the NMR structure of FimC represented by 20 energy-minimized DYANA conformers. The superposition is for minimal r.m.s.d. of the backbone atoms N, Cα and C' of the residues 3–70, 80–90 and 106–116 in the N-terminal domain. **d**, Same as (c), except the superposition for minimal r.m.s.d. is for the backbone atoms of the C-terminal domain with residues 130–203. **e**, Same as (c) with superposition for minimal RMSD of the aforementioned backbone atoms in both domains. In (c)–(e) the residues used for the superposition are colored blue and/or red, where the blue residues are in the N-terminal domain and the red ones in the C-terminal domain.

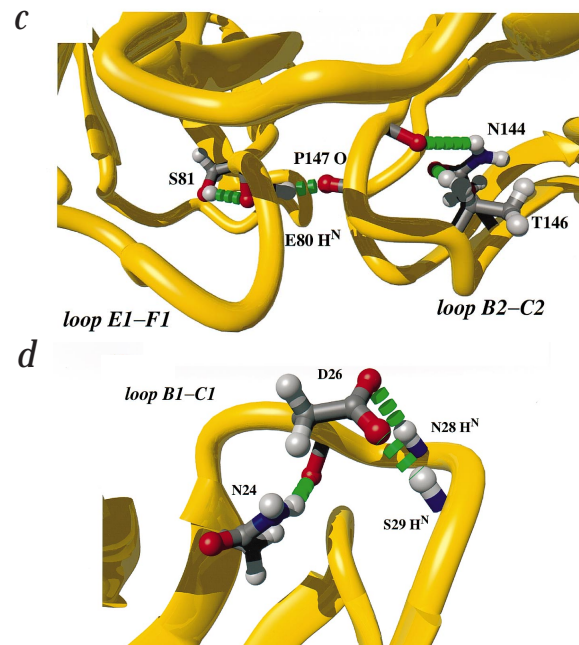
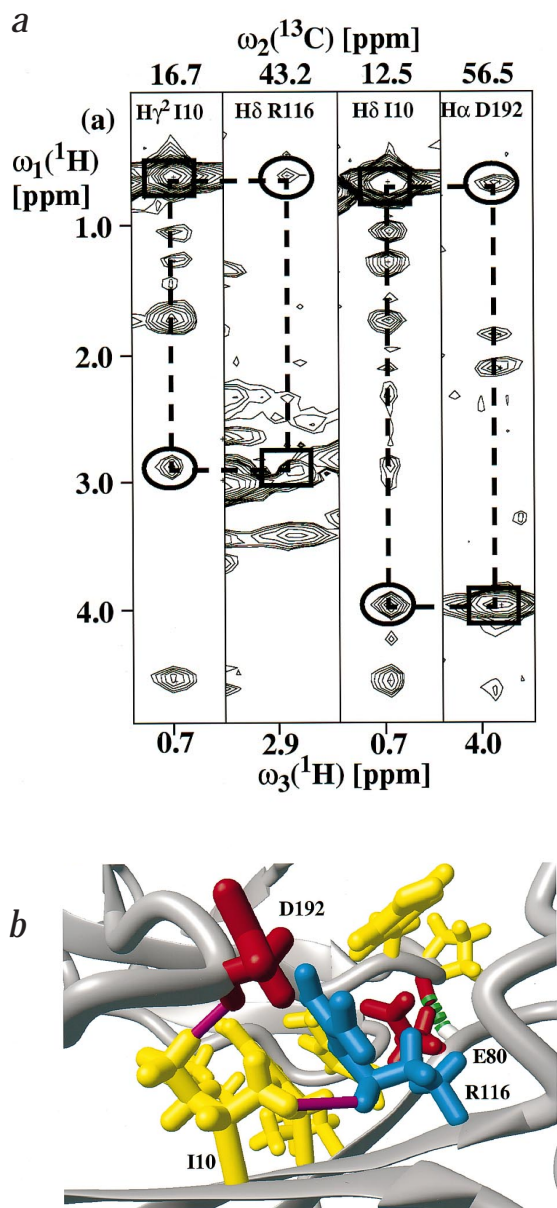


Fig. 2 Interdomain NOEs and interdomain contacts in FimC. **a**, Strips along ω_1 taken from a 3D ^{13}C -resolved $[\text{H}, \text{H}]\text{-NOESY}$ spectrum (mixing time 50 ms). The ellipsoids indicate NOEs of the methyl protons of Ile 10 with δCH_2 of Arg 116 and αH of Asp 192. The broken lines link the NOE cross peaks with the connected diagonal peaks, which are identified by squares. **b**, Interface region between the two domains of FimC. The hydrophobic side chains of Ile 10, Leu 82 and Tyr 114 from the N-terminal domain, and of residues Pro 147, Tyr 148 and Tyr 149 from the C-terminal domain are shown in yellow, and the side chains of Glu 80, Asp 192 and Arg 116, which are involved in an inter-domain salt bridge, are shown in red and blue to represent the negative and positive charges respectively. The inter-domain connectivities corresponding to the NOEs in (a) are indicated by pink lines. An interdomain hydrogen bond formed by the amide proton of Glu 80 and the carbonyl oxygen of Pro 147 is represented by a green broken line. **c**, Residues in the E1-F1 and B2-C2 loops that are involved in intra- and inter-domain interactions through hydrogen bonding. Hydrogen bonds of the backbone amide proton of Glu 80 with the carbonyl oxygen of Pro 147, the hydroxyl proton of Ser 81 with the carboxyl oxygen of Glu 80, a δ amide proton of Asn 144 with the carbonyl oxygen of Tyr 148, and the hydroxyl proton of Thr 146 with the side chain carbonyl oxygen of Asn 144 are shown as green broken tubes. **d**, Hydrogen bonds stabilizing the B1-C1 loop. The hydrogen bonds between an Asn 24 δ proton and the carbonyl oxygen of Asp 26, the side chain carboxylate of Asp 26 and the backbone amide proton of Asn 28, and the side chain carboxylate of Asp 26 and the backbone amide proton of Ser 29 are shown as green broken tubes.

FimC-assisted assembly of type-1 pili on the molecular level, we have determined the three-dimensional structure of FimC from *E. coli* in solution by nuclear magnetic resonance (NMR) spectroscopy.

NMR structure of FimC

FimC consists of a N-terminal domain with residues 1–115 and a C-terminal domain with residues 131–205, which are connected by a linker peptide of 15 amino acid residues (Fig. 1a,b). Both domains have a β -sheet topology that is reminiscent of an immunoglobulin fold, with the first domain containing a barrel-like arrangement of two β -sheets with the strands 2–13, 17–24, 30–38, 48–59, 61–67, 81–92 and 106–115 (A1–G1), and the second domain consisting of a sandwich of two β -sheets formed by the residues 132–135, 138–145, 149–156, 161–167, 170–177, 182–190 and 195–202 (strands A2–G2). The linker peptide (residues 116–130) contains a short 3_{10} -helix of residues 126–130. In the connections between the regular secondary

structure elements, several well defined β -turns consisting of residues 39–42, 68–71, 136–139, 157–160 and 191–194, and a γ -turn consisting of residues 45–47 could be identified. Some other connections are less well ordered due to scarcity of long-range NOEs, including the segment 71–79, the loop F1–G1 and part of the linker peptide. In the bend between the strands D1' and D1'' the peptide bond Thr 51–Pro 52 adopts a *cis* conformation, as manifested by a strong $^1\text{H}\alpha\text{-}^1\text{H}\alpha$ sequential NOE¹². Overall, the two domains are individually very well defined (Table 1; Fig. 1c,d).

The relative arrangement of the two domains is mainly determined by a number of hydrophobic interdomain contacts involving residues Ile 10, Leu 82 and Tyr 114 from the N-terminal domain, and residues Tyr 148, Pro 147 and Tyr 149 from the C-terminal domain (Fig. 2b). In addition, an interdomain salt-bridge linking the residues Arg 116, Glu 80 and Asp 192 contributes to the orientation of the two domains (Fig. 2b). The close proximity of Arg 116 and Asp 192 is also manifested by

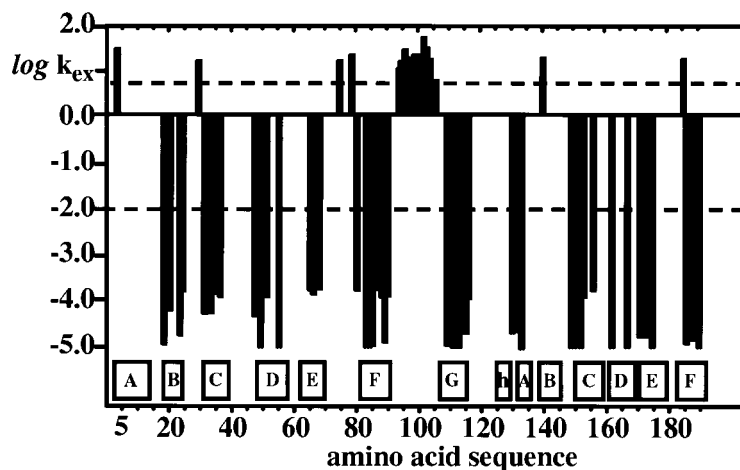


Fig. 3 Logarithmic plot of backbone amide proton exchange rates (s^{-1}) at pH 5.0 and $T = 38^\circ\text{C}$ versus the amino acid sequence of FimC. For all non-proline residues for which the rate is not indicated by a vertical black bar the exchange rate falls between the two dashed horizontal lines, which bound the range of 'intermediate' exchange rates from $10^{-2} s^{-1}$ to $4 s^{-1}$. The locations of regular secondary structures are indicated at the bottom, where the 3_{10} -helix is identified as 'h' and the β -strands in each domain are labeled A–G as in Fig. 1.

NOEs between the methyl protons of Ile 10 and both the δ -protons of Arg 116 and the α -proton of Asp 192 (Fig. 2a). Furthermore, the $^1\text{H}\text{e}-^{13}\text{N}$ correlation of Arg 116, as well as the side chain $^1\text{H}\beta-^{13}\text{C}\text{O}\gamma$ correlation of Asp 192 give broadened weak signals and show large shifts that are typical of hydrogen bond or salt bridge formation^{13,14}. An additional interdomain interaction is represented by a hydrogen bond involving the backbone amide proton of Glu 80 and the carbonyl oxygen of Pro 147, which results from contact of the loop E1-F1 in the N-terminal domain with the loop B2-C2 in the C-terminal domain (Fig. 2c). The relative positioning of these two loops is further determined by a complex hydrogen bond network that involves the side chains of residues Ser 81, Asn 144 and Thr 146, where the Asn 144 side chain is involved in hydrogen bonds with the backbone carbonyl oxygen of Tyr 148 and the γ -proton of Thr 146 (Fig. 2c). Although the relative orientation of the two domains is less precisely defined than the structures of the individual domains (Table 1; Fig. 1e), these interactions result in a unique positioning of the two domains relative to each other (Fig. 1a,e).

There are also numerous 'non-regular' hydrogen bonds in the architecture of the individual domains. An illustration is the link of a δ -proton of Asn 24 with the carbonyl oxygen of Asp 26 in the loop B1-C1, which is further stabilized by hydrogen bonds between the side chain carboxylate of Asp 26 and the backbone amide protons of Asn 28 and Ser 29 (Fig. 2d).

In addition to the NOE connectivities, amide proton exchange studies^{12,15} were used to characterize the hydrogen bonds. The backbone amide proton exchange rates (Fig. 3) correlate well with the hydrogen bonding patterns in the NMR structure of FimC, with the sole exceptions that the residues in the β -strands A1, B2 and G2 exchange with intermediate rather than slow rates. Fast exchange was observed for the residues 92–104 in the loop F1-G1, which confirms that this loop is solvent-exposed in solution (Fig. 1a). A particular situation is observed for the backbone amide protons of Asn 28 and Ser 29, which are hydrogen-bonded with the side chain carboxylate of Asp 26 and exchange with intermediate and fast rates respectively (Fig. 3), which is possibly due to a catalytic effect of the Asp 26 carboxylate. The side chain amide protons of Asn 24 and Asn 144, which are involved in buried hydrogen bonds (Fig. 2c,d), are among the slowly exchanging protons. The interdomain hydrogen bond between the amide proton of Glu 80 and the carbonyl oxygen of Pro 147 (Fig. 2b,c) is also mani-

festated by slow exchange of the backbone amide proton of Glu 80 (Fig. 3).

Comparison to other periplasmic chaperones

The present view of chaperone-assisted pilus assembly is mainly based on structural and functional studies of PapD, which is the periplasmic chaperone of P-pili from *E. coli*^{6,11,16,17} and shares 34% sequence identity with FimC. A crystal structure of PapD has been determined at 2.5 Å resolution¹¹. The average pairwise root-mean-squared deviation (r.m.s.d.) values after superposition of the backbone heavy atoms of the residues that form the β -strands in the 20 individual conformers of the NMR structure of FimC with the corresponding atoms in the crystal structure of PapD are 1.2 Å for the N-terminal domain and 1.6 Å for the C-terminal domain. The r.m.s.d. value is 3.1 Å when both domains are superimposed for best fit (Fig. 4a–c). When compared to the very close similarity of the N-terminal domains (Fig. 4a) there are more extensive differences between the C-terminal domains, where PapD has an additional β -strand (H2) and an insertion of five amino acid residues in the loop between the β -strands C2 and D2 (Fig. 4b,d). The relative domain orientation is also somewhat different in the two proteins (Fig. 4c).

Sequence alignment of FimC and PapD, and a consensus sequence derived from comparison of 17 members of this chaperone family⁷ (Fig. 4d) show that most of the residues that are conserved between FimC and PapD belong to the hydrophobic core of either of the two domains (Fig. 1), or have another essential role in defining the three-dimensional structure of the molecule. For example, the conserved residue Pro 52, which adopts a *cis*-peptide bond, induces and maintains a bend that splits strand D1 in the N-terminal domain into two 'half-strands', which belong to different β -sheets (Fig. 1a,b). The residues Asn 24 and Asn 144 are involved in the positioning of the loops B1-C1 and B2-C2 respectively (Fig. 2c,d), and the side chain of Thr 174 forms an interstrand hydrogen bond with Thr 141 that connects the β -strands E2 and B2. The conserved residues Ile 10, Leu 82, Tyr 114 and Tyr 148 form a small hydrophobic core between the two domains (Fig. 2b), and the conserved residues Arg 116, Asp 192 and Glu 80 form an interdomain salt bridge (Fig. 2b). Overall, the sequence distribution of conserved residues in periplasmic chaperones and their locations in the structures of FimC and PapD suggest a common

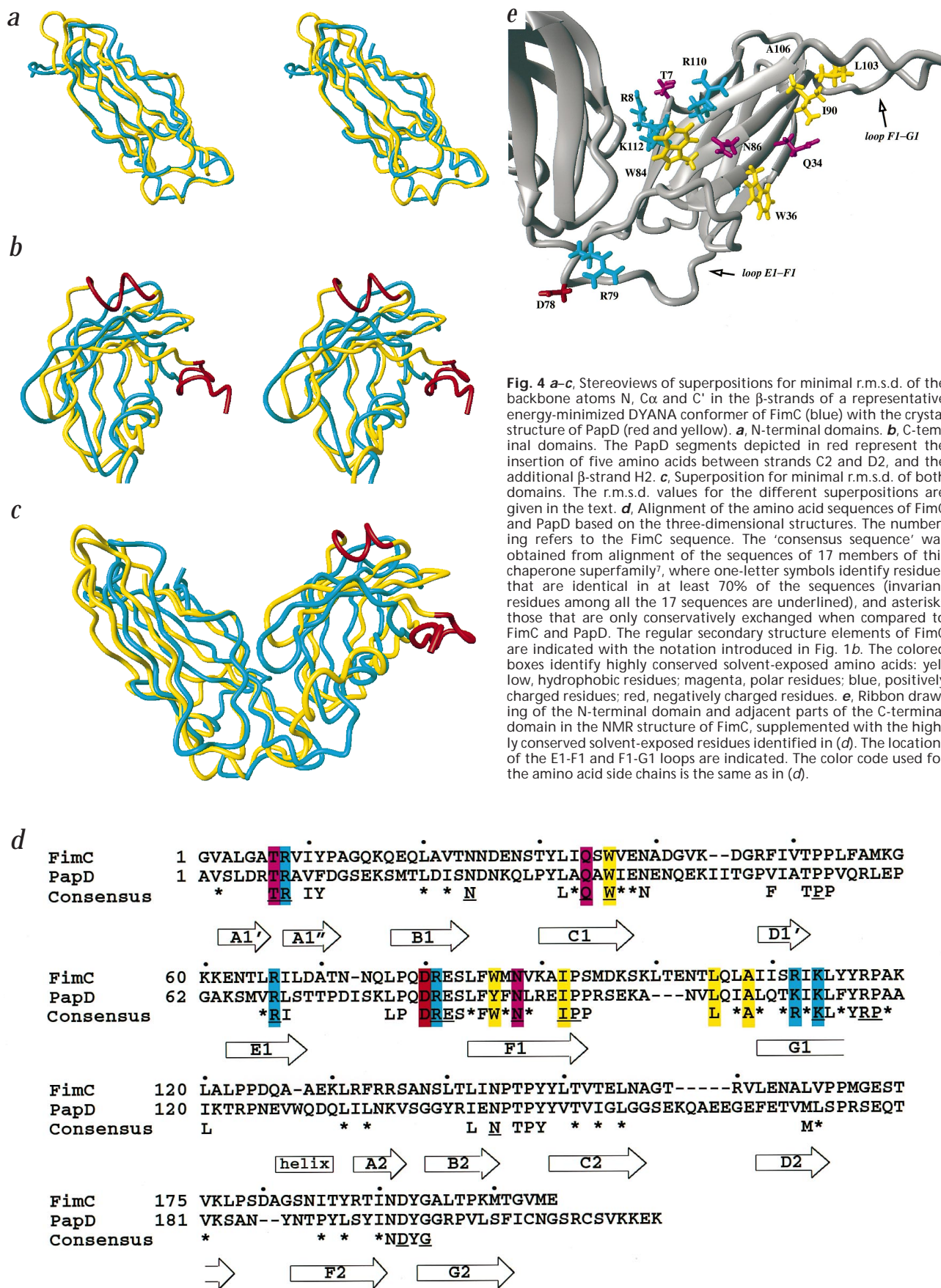


Fig. 4 a-c, Stereoviews of superpositions for minimal r.m.s.d. of the backbone atoms N, C α and C' in the β -strands of a representative energy-minimized DYANA conformer of FimC (blue) with the crystal structure of PapD (red and yellow). **a**, N-terminal domains. **b**, C-terminal domains. The PapD segments depicted in red represent the insertion of five amino acids between strands C2 and D2, and the additional β -strand H2. **c**, Superposition for minimal r.m.s.d. of both domains. The r.m.s.d. values for the different superpositions are given in the text. **d**, Alignment of the amino acid sequences of FimC and PapD based on the three-dimensional structures. The numbering refers to the FimC sequence. The 'consensus sequence' was obtained from alignment of the sequences of 17 members of this chaperone superfamily⁷, where one-letter symbols identify residues that are identical in at least 70% of the sequences (invariant residues among all the 17 sequences are underlined), and asterisks those that are only conservatively exchanged when compared to FimC and PapD. The regular secondary structure elements of FimC are indicated with the notation introduced in Fig. 1b. The colored boxes identify highly conserved solvent-exposed amino acids: yellow, hydrophobic residues; magenta, polar residues; blue, positively charged residues; red, negatively charged residues. **e**, Ribbon drawing of the N-terminal domain and adjacent parts of the C-terminal domain in the NMR structure of FimC, supplemented with the highly conserved solvent-exposed residues identified in (d). The locations of the E1-F1 and F1-G1 loops are indicated. The color code used for the amino acid side chains is the same as in (d).

three-dimensional fold for all pilus chaperone proteins identified so far.

Specificity of FimC interactions

Initial insight into the molecular basis of chaperone–pilus subunit interactions was derived from a crystal structure at 3.0 Å resolution of PapD complexed with a synthetic peptide with the sequence of the 19 C-terminal residues of a P-pilus subunit⁶. The C-terminal carboxylate group of this peptide is bound to the invariant residues Arg 8 and Lys 112 in the cleft between the two domains, and the peptide further interacts with the β-strand G1 and part of the F1-G1 loop of PapD⁶. The critical role of Arg 8 and Lys 112 in PapD for the binding of pilus subunits implicated by this structural model was further evidenced by studies of the two variants PapD(R8A) and PapD(K112A), which are no longer capable of mediating the assembly of P-pili⁶. Arg 8, Lys 112 and all other solvent-exposed residues that are conserved between PapD and FimC (Fig. 4d) are located in the N-terminal domain (Fig. 4e), where they are likely to have functional roles in the interactions with the pilus subunits. The large number of conserved surface residues between FimC and PapD in the peptide binding area of the N-terminal domain may confer a certain degree of promiscuity to the process of pilus subunit recognition. Indeed, certain subunits of F1C and type-1 pili have been shown to be exchangeable between the pili, so that hybrid pili are formed¹⁸, suggesting that the ability of the chaperones to recognize subunits from their own pilus system is not especially pronounced. Some specificity of the binding process may come from structural differences far distant from the peptide binding site, for example, the loop C1-D1' with residues 39–47 is strongly variable among related periplasmic chaperones, both in the residue types and the length of the loop (-1 to +5 residues compared to FimC)⁷ (Fig. 4d). The succession of a β-turn and γ-turn in the C1-D1' loop of FimC may thus confer a certain specificity for type-1 pilus subunit recognition.

Presently 26 different adhesive pilus systems are known from various Gram-negative pathogenic bacteria⁷. Each of these different pilus systems contains its own periplasmic chaperone and its own assembly platform. The fact that different pili co-exist independently in *E. coli* suggests that each chaperone selectively interacts with its own assembly platform. This view is supported by complementation experiments with the assembly platforms and the chaperones of type-1, and the F1C pili from *E. coli*. Although FimC cannot functionally substitute for FocC (the related chaperone from F1C pili), or *vice versa*, combined substitution of the chaperone/assembly platform systems works both ways¹⁹. In addition, FimC is not capable of complementing PapD deficiency⁴, whereas, in apparent contrast with all other data, PapD has been reported to complement FimC deficiency (it cannot, however, be ruled out that this diverging result may be due to strong overexpression of PapD in the complementation assay⁴).

Clearly, the chaperone-mediated assembly of adhesive pili must depend critically on specific assembly platform recognition by these chaperones to ensure that the pilus subunits are released to the correct assembly platform. The comparison of the structures of FimC and PapD (Fig. 4a–d) reveals significant differences in the backbone fold and surface properties of the C-terminal domains of FimC and PapD, which could provide suitable targets for pilus-specific assembly platform interactions. This would suggest that interaction of the C-terminal chaperone domain with the assembly platform is critical for the

Table 1 Characterization of the energy-minimized NMR structure of FimC¹

Quantity	20 conformers ²
Residual distance constraint violations	
Number ≥ 0.1 Å	0.6 ± 0.7
Maximum (Å)	0.10 ± 0.01
Residual dihedral angle constraint violations	
Number ≥ 2.5°	0.4 ± 0.6
Maximum (°)	2.4 ± 0.2
AMBER energies (kcal mol ⁻¹)	
Total	-8,303 ± 64
Van der Waals	-667 ± 18
Electrostatic	-9,334 ± 68
R.m.s. deviation from ideal geometry	
Bond lengths (Å)	0.0072 ± 0.0001
Bond angles (°)	2.07 ± 0.02
Peptide bonds (°)	10.3 ± 0.5
R.m.s.d. to the averaged coordinates ³ (Å)	
N, Cα, C' (3–70, 80–90, 106–116)	0.68 ± 0.12
N, Cα, C' (130–203)	0.56 ± 0.09
N, Cα, C' (3–70, 80–90, 106–116, 130–203)	1.03 ± 0.35
All heavy atoms (3–70, 80–90, 106–116, 130–203)	1.43 ± 0.34

¹NMR spectra were recorded with an aqueous solution containing 1.0 mM of FimC, pH = 5.0, T = 38 °C. The input for the structure calculation consisted of 1,967 NOE upper distance limits (661 intraresidual, 544 sequential, 152 medium-range, 604 long-range) and 452 dihedral angle constraints (174 for φ, 174 for ψ, 104 for χ¹). The average residual target function value for the 20 best DYANA conformers before energy minimization was 1.95 ± 0.24 Å².

²For each entry the average for the 20 conformers with the lowest residual DYANA target function values and the variation among the 20 conformers are given.

³Average coordinates of the 20 energy-minimized conformers after superposition for best fit of the N, Cα and C' atoms of the residues indicated in parentheses.

release of the subunits to the growing pilus. The presently proposed view of complementary tasks of the N- and C-terminal domains of periplasmic pilus chaperones is also supported by the finding that a chimeric PapD/FimC chaperone consisting of residues 1–112 of PapD and residues 113–205 of FimC is not capable of mediating assembly of either type-1 or P-pili²⁰. Additional experiments which show that binding of chaperone-subunit complexes to an assembly platform *in vitro* does not result in release of the pilus subunit²¹, suggest further that the assembly of bacterial pili *in vivo* may also involve additional proteins in a complex multimolecular process²², within the context of which the presently invoked separate functions of the two chaperone domains would presumably have an important role.

The information obtained from comparison of the three-dimensional structures of FimC and PapD is an important step towards understanding the general mechanistic features underlying the function of bacterial pilus chaperones. It enhances the potential role of either of the two structures as starting points for the long-term goal of designing novel therapeutics against Gram-negative bacteria, in the case of FimC specifically of drugs against uropathogenic *E. coli* strains that would inhibit assembly of type-1 pili.

Methods

Sample preparation. For the production of uniformly ¹⁵N-labeled, ¹³C/¹⁵N-doubly-labeled, and 10% ¹³C biosynthetically-directed labeled FimC, cells of *E. coli* BL21(DE 3) harboring the

expression plasmid pFimC (U. Hermans, P. Sebbel, V. Eggli and R. Glockshuber, in preparation) were grown at 25 °C in 10 l minimal medium containing ($^{15}\text{NH}_4$) $_2\text{SO}_4$ (1.5 g l $^{-1}$) and either unlabeled glucose (5 g l $^{-1}$), [$^{13}\text{C}_6$]-glucose (2 g l $^{-1}$), or a mixture of 90% unlabeled glucose (4.5 g l $^{-1}$) and 10% of [$^{13}\text{C}_6$]-glucose (0.5 g l $^{-1}$).

NMR data collection and structure calculation. The NMR structure determination of FimC was performed with 1 mM solutions in 90% H $_2$ O/10% D $_2$ O at pH 5.0 and 38 °C, which is well below the melting point of the protein (63.5 °C). Light scattering measurements showed that the protein is monomeric under these conditions. On the basis of the resonance assignments obtained for FimC 23 , a total of 4,512 NOE cross peaks were assigned and integrated, using 3D ^{15}N -resolved [$^1\text{H},^1\text{H}$]-NOESY, 3D ^{13}C -resolved [$^1\text{H},^1\text{H}$]-NOESY and 2D [$^1\text{H},^1\text{H}$]-NOESY, which were recorded at 750 MHz with a mixing time of 50 ms. In addition, 120 $^3J_{\text{HN}\alpha}$ coupling constants were determined by inverse Fourier transformation of in-phase multiplets from a 2D [$^{15}\text{N},^1\text{H}$]-COSY spectrum 24,49 $^3J_{\text{NH}}$ coupling constants were estimated from 3D ct-HNNHB 25,26 and 38 $^3J_{\text{O}\beta}$ coupling constants were derived from a 3D HACAHB-COSY spectrum 27 . The input for calculation of the FimC structure with the program DYANA 28 consisted of upper distance limits derived from NOESY cross peak intensities, as described in ref. 29, and of dihedral angle constraints derived from the combination of the above-mentioned $^3J_{\text{HN}\alpha}$, $^3J_{\text{O}\beta}$ and $^3J_{\text{NH}}$ coupling constants with intraresidual and sequential NOEs 12 , using the program HABAS 30 . Several rounds of structure calculation with DYANA 28 and NOESY cross peak assignment with the program ASNO 31 were performed. Stereospecific assignments were obtained with the programs HABAS 30 and GLOMSA 29 for 6 out of 11 α -CH $_2$ groups, 51 out of 137 β -CH $_2$ s, and 2 out of 41 γ -CH $_2$ s. Individual proton assignments for 21 of the 22 NH $_2$ groups of Asn and Gln were also obtained. Stereospecific assignments for 9 out of 12 Val γ -CH $_3$ s and for 14 out of 22 Leu δ -CH $_3$ s were obtained by biosynthetically-directed fractional ^{13}C labeling 32,33 and 2D [$^{13}\text{C},^1\text{H}$]-COSY. After removal of irrelevant NOEs and processing of constraints with non-stereospecifically assigned diastereotopic protons with the program DYANA 28 , a final data set of 1,961 NOE upper distance limits (661 intraresidual, 544 sequential, 152 medium-range, 604 long-range) and 452 dihedral angle constraints (174 for ϕ , 174 for ψ , 104 for χ_1) was obtained and used as input for the structure calculation with the torsion angle dynamics algorithm implemented in the program DYANA 28 , which was followed by energy minimization with the program OPAL 34 . In the results of the structure calculation (Table 1) the small size and small numbers of residual constraint violations show that the input data form a self-consistent set, and that the constraints are well satisfied in the 20 conformers used to represent the solution structure of FimC.

With a final input of 1,961 NOE upper distance limits and 452 dihedral angle constraints the standard DYANA simulated annealing protocol 28 was used with 12,000 torsion angle dynamics steps, where the bond lengths and bond angles were fixed at standard values throughout the calculation. The final round of DYANA structure calculations was started with 80 randomized conformers. As usual 12,28,29 , the 20 DYANA conformers with the lowest residual target function values (Table 1) were subjected to restrained energy minimization in Cartesian space, using the standard AMBER all-atom force field as implemented in the program OPAL 34 . The restrained energy minimization was carried out in a shell of water molecules with a minimal thickness of 6 Å, performing a total of 1,500 steps of conjugate gradient minimization for each conformer. The dielectric constant was 1, and no cutoff for non-bonded interactions was applied. The resulting 20 energy-refined conformers are used to represent the solution structure of FimC.

Coordinates. The atomic coordinates of the energy-minimized structure of FimC have been deposited with the Brookhaven Protein Data Bank (accession number 1BF8).

Acknowledgments

We thank V. Eggli for assistance with the preparation of FimC and S. Knight for providing us with coordinates of PapD and a PapD-peptide complex. Financial support was obtained from the Schweizerischer Nationalfonds to K.W. and R.G., and from an EMBO fellowship to M.P.

Maurizio Pellecchia 1,2 , Peter Güntert 1 , Rudi Glockshuber 1 and Kurt Wüthrich 1

1 Institut für Molekularbiologie und Biophysik, Eidgenössische Technische Hochschule Hönggerberg, CH-8093 Zürich, Switzerland. 2 Present address: Biophysics Research Division, The University of Michigan, 930 North University Avenue, Michigan 48109, USA.

Correspondence should be addressed to R.G. email: rudi@mol.biol.ethz.ch or K.W. fax: 41 1 6331151.

Received 1 June, 1998; accepted 6 August, 1998.

- Hultgren, S.J., Jones, C.H. & Normark, S. In *Escherichia coli and Salmonella. Cellular and molecular biology*. (ed. Neidhardt, F.E.) 2730–2756 (ASM Press, Washington, DC, 1996).
- Hultgren, S.J., Abraham, S., Caparon, M. & Falk, P. *Cell* **73**, 887–901 (1993).
- Boarto, D.M. *et al. Nature* **389**, 636–639 (1997).
- Jones, C.H. *et al. Proc. Natl. Acad. Sci. USA* **90**, 8397–8401 (1993).
- Klemm, P. *Res. Microbiol.* **143**, 831–838 (1992).
- Kuehn, M.J. *et al. Science* **262**, 1234–1241 (1993).
- Hung, D.L., Knight, S.D., Woods, R.M., Pinker, J.S. & Hultgren, S.J. *EMBO J.* **15**, 3792–3805 (1996).
- Harti, F.U. *Nature* **381**, 571–580 (1996).
- Connell, H. *et al. Proc. Natl. Acad. Sci. USA* **93**, 9827–9832 (1996).
- Langermann, S. *et al. Science* **276**, 607–611 (1997).
- Holmgren, A., & Brändén, C.I. *Nature* **342**, 248–251 (1989).
- Wüthrich, K. *NMR of proteins and nucleic acids*. (Wiley, New York, 1986).
- Pascal, S.M., Yamazaki, T., Singer, A.U., Kay, L.E. & Forman-Kay, J.D. *Biochemistry* **34**, 11353–11362 (1995).
- Feng, M.F. & Dyson, H. J. *Biochemistry* **35**, 1–6 (1996).
- Gemmeker, G., Jahnke, W. & Kessler, H. *J. Am. Chem. Soc.* **115**, 11620–11621 (1993).
- Kuehn, M.J., Normark, S. & Hultgren, S.J. *Proc. Natl. Acad. Sci. USA* **88**, 10586–10590 (1991).
- Holmgren, A., Kuehn, M.J., Branden, C.I., & Hultgren, S.J. *EMBO J.* **11**, 1617–1622 (1992).
- Klemm, P., Christiansen, G., Kreft, B., Marre, R. & Bergmans, H.J. *Bacteriol.* **176**, 2227–2234 (1994).
- Klemm, P., Jorgensen, B.J., Kreft, B. & Christiansen, G.J. *Bacteriol.* **177**, 621–627 (1995).
- Jones, C.H., Danese, P.N., Pinker, J.S., Silhavy, T.J. & Hultgren, S.J. *EMBO J.* **16**, 6394–6406 (1997).
- Dodson, K.D., Jacob-Dubuisson, F., Stiker, R.T. & Hultgren S.J. *Proc. Natl. Acad. Sci. USA* **90**, 3670–3674 (1993).
- Jones, C.H. *et al. Proc. Natl. Acad. Sci. USA* **92**, 2081–2085 (1995).
- Pellecchia, M., Güntert, P., Glockshuber, R. & Wüthrich, K.J. *Biomol. NMR* **11**, 229–230 (1998).
- Szyperski, T., Güntert, P., Otting, G. & Wüthrich, K. *J. Magn. Reson.* **99**, 552–560 (1992).
- Archer, S.J., Ikura, M., Torchia, D.A. & Bax, A. *J. Magn. Reson.* **95**, 636–641 (1991).
- Chary, K.V.R., Otting, G. & Wüthrich, K. *J. Magn. Reson.* **93**, 218–224 (1991).
- Grzesiek, S., Kuboniwa, H., Hinck, A.P. & Bax, A. *J. Am. Chem. Soc.* **117**, 5312–5315 (1995).
- Güntert, P., Mumenthaler, C. & Wüthrich, K. *J. Mol. Biol.* **273**, 283–298 (1997).
- Güntert, P., Braun, W. & Wüthrich, K. *J. Mol. Biol.* **217**, 517–530 (1991).
- Güntert, P., Braun, W., Billeter, M. & Wüthrich, K. *J. Am. Chem. Soc.* **111**, 3997–4004 (1989).
- Güntert, P., Berndt, K.D. & Wüthrich, K. *J. Biomol. NMR* **3**, 601–606 (1993).
- Senn, H. *et al. FEBS Lett.* **249**, 113–118 (1989).
- Neri, D., Szyperski, T., Otting, G., Senn, H. & Wüthrich, K. *Biochemistry* **28**, 7510–7516 (1989).
- Luginbühl, P., Güntert, P., Billeter, M. & Wüthrich, K. *J. Biomol. NMR* **8**, 136–146 (1996).
- Koradi, R., Billeter, M. & Wüthrich, K. *J. Mol. Graphics* **14**, 52–55 (1996).